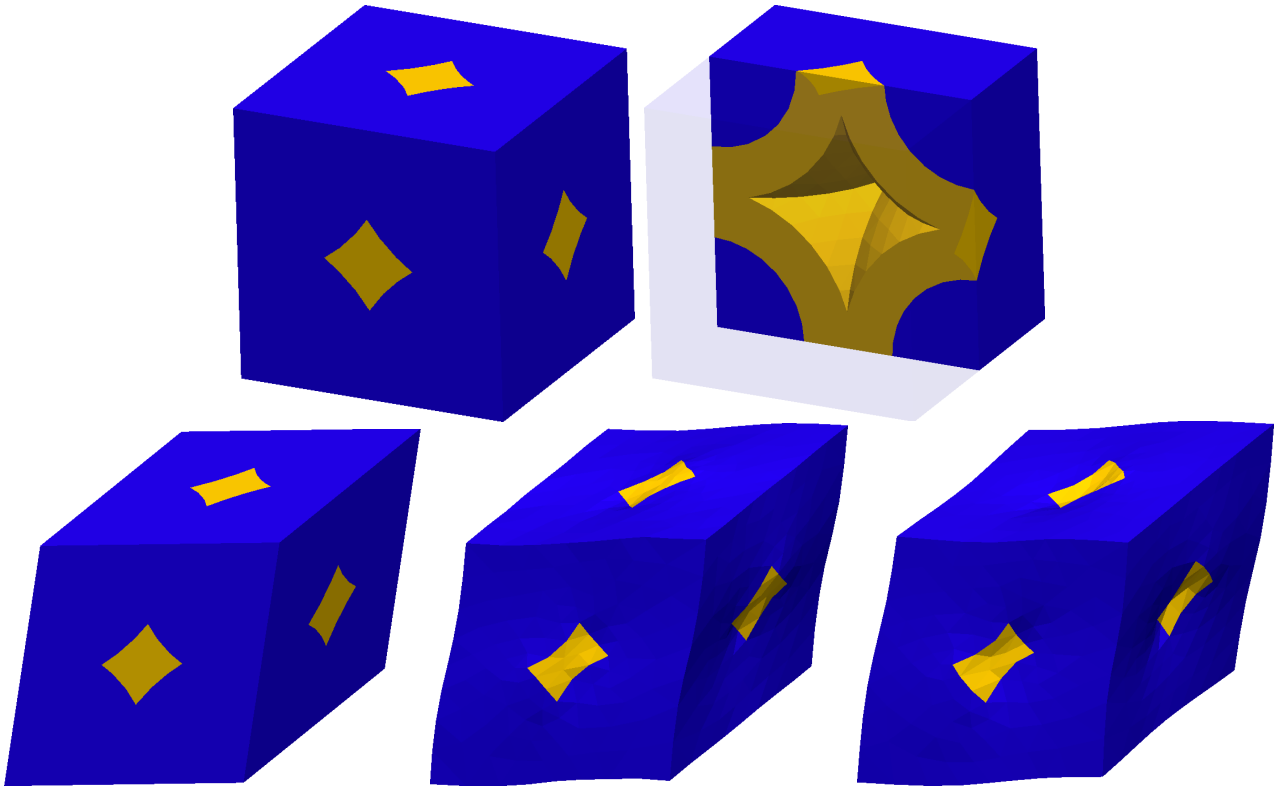

On Computational Modeling of Sintering based on Homogenization

MIKAEL ÖHMAN

Department of Applied Mechanics
CHALMERS UNIVERSITY OF TECHNOLOGY
Göteborg, Sweden 2014

THESIS FOR THE DEGREE OF DOCTOR OF PHILOSOPHY IN SOLID AND STRUCTURAL MECHANICS

On Computational Modeling of Sintering based on Homogenization

MIKAEL ÖHMAN

Department of Applied Mechanics
CHALMERS UNIVERSITY OF TECHNOLOGY

Göteborg, Sweden 2014

On Computational Modeling of Sintering based on Homogenization
MIKAEL ÖHMAN
ISBN 978-91-7597-003-5

Doktorsavhandlingar vid Chalmers tekniska högskola
Ny serie nr. 3684
ISSN 0346-718X
Department of Applied Mechanics
Chalmers University of Technology
SE-412 96 Göteborg
Sweden
Telephone: +46 (0)31-772 1000

Cover:
Representative Volume Element in undeformed state and subjected to shear. Dirichlet, Periodic and Neumann boundary conditions are visualized on the bottom row.

Chalmers Reproservice
Göteborg, Sweden 2014

On Computational Modeling of Sintering based on Homogenization
Thesis for the degree of Doctor of Philosophy in Solid and Structural Mechanics
MIKAEL ÖHMAN
Department of Applied Mechanics
Chalmers University of Technology

Abstract

Liquid-phase sintering is the process where a precompacted powder, "green body", is heated to the point where (a part of) the solid material melts, and the specimen shrinks while keeping (almost) net shape. In the case of hardmetal, the microstructure is defined by WC-Co-particles with large pores, whereby molten Co represents the liquid phase. In the ideal case, a fully dense material is achieved when the sintering is completed. The "driving force" of the sintering procedure is surface tension along the free surfaces, i.e. Co-pore interfaces. In this thesis, the intrinsic deformation of both the solid phase and the melt phase is modeled as the creeping flow of the Stokes' type, whereby elastic deformation is ignored.

The macroscopic properties are derived via computational homogenization that utilizes a highly idealized mesostructure within each Representative Volume Element (RVE). 2D RVE's are used predominantly; however, 3D-mesostructures are also analyzed. Within the FE^2 algorithmic setting, the homogenization is carried out at the Gaussian integration points in the macroscale FE-mesh. This allow for the investigation of properties that are not easily captured with traditional macroscopic constitutive models, which inevitably would become highly complex with many material parameters that lack physical interpretation.

The finite element mesh of the RVE becomes heavily deformed as the surface tension pulls the particles closer; hence, it was necessary to develop a surface tracking method with remeshing. As an element in the mesh reaches a certain deformed state, defined by the condition number of the Jacobian, a new mesh is created.

The FE^2 algorithm has been implemented in the open source FE-code OOFEM (written in C++) where the code is parallelized w.r.t. the elements in the macroscale mesh.

A number of (more generic or less generic) issues related to the homogenization theory and algorithm are discussed in the thesis: (i) The implications of Variationally Consistent Homogenization (VCH) and the consequent satisfaction of the "macrohomogeneity condition". One issue is how to homogenize the stress and volumetric rate-of-deformation when pores are present. (ii) How to establish a variational framework on both scales, based on a suitable mixture of fields, that allows for a seamless transition from macroscopically compressible to incompressible response. Such a transition is of utmost importance for the practical use of the FE^2 algorithm in view of eventual macroscopic incompressibility of each individual RVE (as the porosity vanishes locally). In particular, the corresponding RVE-problems are designed in such a fashion that they are "fed" by the deviatoric part of the macroscopic rate-of-deformation and the macroscopic pressure. (iii) The role of boundary conditions on RVE, in particular how bounds on the "macroscale energy density" can be established via the use of Dirichlet and Neumann boundary conditions. Numerical examples are shown for different loading scenarios, where the macroscopic behavior is studied.

Keywords: Liquid phase sintering, Incompressibility, Mixed variational formulations, Multi-scale, Computational homogenization, FE^2

Preface

The work presented in this thesis was carried out at the division of Material and Computational Mechanics at Chalmers University of Technology during 2009–2014. It was funded by the Swedish Research Council.

I would like to thank my supervisor Professor Kenneth Runesson and my co-supervisor Professor Fredrik Larsson for their valuable guidance and help with technical expertise. My fellow Ph.D. students have also spent a lot of time discussing and helping me when problems arose. I could not hope for better friends and coworkers.

Göteborg in May, 2014
Mikael Öhman

Nomenclature

RVE Representative Volume Element

VCH Variationally Consistent Homogenization

VCMC Variationally Consistent Macrohomogeneity Condition

$\bullet_{\mathrm{d}}$ Subscript d represents deviatoric part of a 2nd order tensor

$\bar{\bullet}$ Bar represents macroscopic variables

$\bullet^{\mathrm{M}}$ Superscript M represents the local prolongation of the macroscopic fields

$\bullet^{\mathrm{s}}$ Superscript s represents fluctuation fields

$\hat{\bullet}$ Hat denotes a constitutive law

$f\{\bullet\}$ Curly brackets are used for implicit functions

$\langle\bullet\rangle_{\square}$ Volume average over particles

$\langle\!\langle\bullet\rangle\!\rangle_{\square}$ Volume average over pore surface

$\boldsymbol{v}$ Velocity

p Pressure

e Volumetric rate of deformation ($\boldsymbol{d}:\boldsymbol{I}$)

$\boldsymbol{d}$ Rate of deformation = symmetric part of the velocity gradient ($[\boldsymbol{v}\otimes\boldsymbol{\nabla}]^{\mathrm{sym}}$)

$\boldsymbol{\sigma}$ Cauchy stress

$\bar{\mathsf{E}} \overset{\mathrm{def}}{=} \dfrac{\partial\,\bar{\boldsymbol{\sigma}}}{\partial\bar{\boldsymbol{d}}}$

$\bar{\mathsf{E}}_{\mathrm{d}} \overset{\mathrm{def}}{=} \dfrac{\partial\,\bar{\boldsymbol{\sigma}}_{\mathrm{d}}}{\partial\bar{\boldsymbol{d}}_{\mathrm{d}}}$

$\bar{\boldsymbol{E}}_{\mathrm{p}} \overset{\mathrm{def}}{=} \dfrac{\partial\,\bar{\boldsymbol{\sigma}}_{\mathrm{d}}}{\partial\bar{p}}$

$\bar{\boldsymbol{C}}_{\mathrm{d}} \overset{\mathrm{def}}{=} \dfrac{\partial\,\bar{e}}{\partial\bar{\boldsymbol{d}}_{\mathrm{d}}}$

$\bar{C}_{\mathrm{p}} \overset{\mathrm{def}}{=} -\dfrac{\partial\,\bar{e}}{\partial\bar{p}}$

Thesis

This thesis consists of an extended summary and the following appended papers:

Paper A M. Öhman, K. Runesson, and F. Larsson. Computational mesoscale modeling and homogenization of liquid-phase sintering of particle agglomerates. *Technische Mechanik* **32** (2012), 463–483. ISSN: 0232-3869. URL: http://www.uni-magdeburg.de/ifme/zeitschrift_tm/2012_Heft2_5/33_Oehman.pdf

Paper B M. Öhman, K. Runesson, and F. Larsson. Computational homogenization of liquid-phase sintering with seamless transition from macroscopic compressibility to incompressibility. *Computer Methods in Applied Mechanics and Engineering* **266** (2013), 219–228. ISSN: 0045-7825. DOI: 10.1016/j.cma.2013.07.006

Paper C M. Öhman, K. Runesson, and F. Larsson. On the variationally consistent computational homogenization of elasticity in the incompressible limit. *Advanced Modeling and Simulation in Engineering Sciences* (2014). Submitted

Paper D M. Öhman. A mixed variational format for two-scale analysis of liquid-phase sintering based on variationally consistent homogenization (2014). In preparation

Papers A–C were prepared in collaboration with the co-authors. The author of this thesis was responsible for the major progress of the work in preparing the papers, i.e. took part in planning the papers, took part in developing the theory, developed the numerical implementation and carried out the numerical simulations.

Contents

Part I
Extended Summary

1 Introduction

1.1 The process of sintering of hardmetal

Manufacturing of PM products is based on the "welding" (sintering) of particles due to heating or combined heating and mechanical loading (uniaxial or isotropic pressing). To model and simulate the sintering of hard metals, often including some form of binder metal, is particularly challenging in view of the fact that the sintering process involves both solid and melt states of the constituents. In brief, the manufacturing process can be split into three different sequential stages: (I) Compaction of powder compound, with initially around 70 % porosity, into a "green body" with roughly 20 % to 40 % porosity. (II) Heating in oven up well above the melting temperature for the binder. (III) Cooling to room temperature. As an example, Co is the binder metal (with melting temperature around 1500 °C) in the system WC-Co-Ti.

The purpose is to achieve net-shape already of the green body, whereby the subsequent sintering would result mainly in change of volume (without distortion, i.e. shear deformation). Since uniaxial pressing is normally used for the initial compaction of hard metal, it is likely that wall friction leads to inhomogeneous distribution of residual stresses and bulk density in the green body (at least to some extent). This is an unwanted effect that obscures the goal of net-shape.

During the heating phase, thermal expansion is combined with a certain amount of solid state sintering before melting of the binder, which is necessary in order to achieve "liquid-phase" sintering. During the hold-time at the given temperature, significant compaction (densification, consolidation) takes place due to a combination of solid deformation, diffusion and liquid motion, which brings about reduced porosity. The so-called "sintering stress", which is a macro-scale manifestation of the surface tension between the constituents and the pores, is the "driving force" for compaction; hence, sintering can take place under zero external load of the specimen (known as "free sintering"). However, the residual stresses after compaction will effect the process.

Clearly, the aim of the process is that the final product is completely dense, i.e. there is no rest-porosity, with no net-shape distortion. This may be hard to accomplish if the green body bulk density is severely inhomogeneous and/or the liquid phase sintering is inefficient (in terms of insufficient amount of binder phase and/or incomplete melting).

1.2 Modeling and simulation efforts — A brief review

A wealth of literature deals with the modeling and simulation of the sintering process. Primarily, this relates to the constitutive modeling of (1) the powder material response for green body (pre)compaction and (2) the high temperature response and sintering mechanisms pertinent to both solid and liquid phase sintering. Modeling efforts can be classified by two major paradigms: *a priori macroscale modeling* and *micromechanics modeling and computational*

homogenization.

1.2.1 Macroscale modeling

A vast majority of the existing literature on *a priori* macro-scale modeling is devoted to the compaction stage, and it is noted that very few (if any) attempts have been made to develop a unifying macroscopic constitutive model for the compaction and sintering stages. As to the compaction process, material rate-independence (elasto-plasticity) is a common (and valid) assumption. Such plasticity models are often taken, at least conceptually, from soil mechanics. The major focus is on the evolution of the yield surface due to changing porosity as the predominant hardening mechanism, e.g. Fleck et al. [FKM92], Oliver et al. [OOC96], Brandt and Nilsson [BN98], Redanz [Red98], Kraft [Kra03].

For the solid phase sintering, the major feature is the strong rate-dependence close to, and above, the melting temperature of the binder. Models based on viscoelasticity and viscoplasticity have, therefore, been proposed to simulate the creep behavior of the highly deformable (and even partly melt) binder, e.g. Shinagawa [Shi96], Brandt and Nilsson [BN98]. Clearly, it is of utmost importance to model the high sensitivity of yield stress to temperature, e.g. Mähler et al. [MR00]. The task of providing a rational thermodynamic definition of the sintering stress was addressed by, e.g. Reid and Oakberg [RO90], Mähler and Runesson [MR03].

As to liquid phase sintering, the text-book by German [Ger96] is still an authority in the field. Examples of the rich literature are Svoboda et al. [SRG96], Xu and Mehrabahdi [XM97], Lu et al. [Lu+01], who used a single-phase approach. In the work by Olevsky and German [Ole98], [OG00] we find the modeling of sintering by a linear viscous material model.

Common to these macroscopic models, which are often of quite complex nature with a large number of model parameters, is the need for calibration from experimental data. Access to such data for various loading scenarios and environmental conditions thus sets the limit of the predictive capabilities.

1.2.2 Micromechanics modeling and computational homogenization

Most micromechanically based models consider idealized geometrical arrangement, such as a regular array of spheres, within a Representative Volume Element (RVE). One common approach is to consider grain boundary diffusion, e.g. Helle, et al. [HEA85], McMeeking and Kuhn [MK92], Riedel and Svoboda [RS93] and Shinagawa [Shi96] and particle bridging via diffusion, e.g. Svoboda and Riedel [SR95], Bient [Bie+04], Luque et al. [Luq+05], as the principal mechanisms for densification. In the recent work by Pino-Muñoz et al. [Pin+13] the modeling of multiple spherical particles is based on a level-set description and accounts for volume and surface diffusion.

Early attempts to numerically simulate the surface-tension driven reshaping of contacting particles are by Jagota and Dawson [JD88a; JD88b] and van de Vorst [Vor93]. In a series of papers, Zhou and Derby [ZD98; ZD01] emphasize efficient finite element algorithms to trace the complex 3-dimensional flow of multi-particle interaction. The main challenges are the complex subscale geometry and the moving free boundary giving rise to very large deformations and severe topology changes. Recent developments of free-boundary tracing FE-strategies for large deformations (without severe topological changes) are discussed by Perić and coworkers, [DP06], [SP06a], [SP06b]. All the mentioned work consider surface tension effects in fluids. A

recent extension to include surface tension in the context of solid modeling, where anisotropic surface energy may be present, is due to Javili and Steinmann [JS10].

Micro-mechanical analysis must be accompanied by computational homogenization in order to obtain a predictive model for a component. In selected references for homogenization we find Nemat-Nasser and Hori [NH93], Geers et al. [GKB10], and Larson et al. [LRS10]. One possibility is socalled upscaling, i. e. to use the subscale modeling to calibrate a macroscopic model. A more appealing, but theoretically and computationally more challenging, possibility is to carry out full-fledged simultaneous coupling between the micro- and macro-scales, which is known as Computational Multiscale Modeling, or the FE^2 strategy, cf. Feyel et al. [FC00]. This is certainly the current international trend in material modeling for engineering purposes; however, to our knowledge no work on the fully coupled FE^2 applied to the sintering problem has been published.

2 Aim and Scope of Research

The thesis concerns the development of a predictive tool for the computational modeling of sintering of hardmetal, that involves a liquid (melt binder) phase. Virtually all modeling in the literature aiming for quantitative predictions on the engineering scale is based on *a priori* homogenized macroscopic material models. In this dissertation, the purpose is rather to obtain the relevant equations via micromechanical modeling and computational homogenization.

In order to achieve the goal, the following tasks are identified:

- Develop the micro-mechanical relations for an ideal setting of viscous particles in contact that sinter due to surface tension.
- Use computational homogenization and a fully coupled FE^2 strategy to obtain a predictive model.
- Develop FE-software, in particular for efficient implementation of parallel algorithms.

3 The fine-scale model problem

3.1 Mixed velocity-pressure formulation

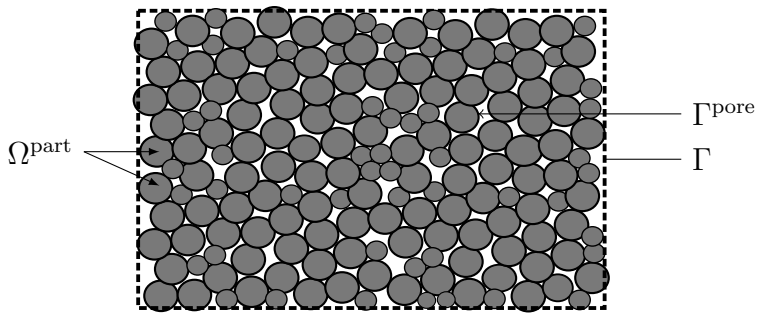

Figure 3.1: *Green body with its macroscopic shape as dashed line. Particles are not to scale.*

We consider a generic micro-heterogeneous material in a given "green body", whose macroscopic configuration occupies the region Ω in space with (presumed smooth) boundary Γ as seen in Figure 3.1. However, the actual medium has pores, which means that the particle composite occupies only the region Ω^{part}. This configuration is illustrated in Figure 4.1. In this setting, the instantaneous velocity field $\boldsymbol{v}$ is solved for at any given time, and explicit time-integration is used to drive the deformations.

We consider a model material as follows: The stress is decomposed in terms of deviator and pressure as $\boldsymbol{\sigma} = \boldsymbol{\sigma}_{\text{d}} - p\boldsymbol{I}$. With the kinematic definition $\boldsymbol{\epsilon}_{\text{d}}[\boldsymbol{v}] \stackrel{\text{def}}{=} [\boldsymbol{v} \otimes \boldsymbol{\nabla}]^{\text{sym}} - \frac{1}{3}[\boldsymbol{v} \cdot \boldsymbol{\nabla}]\boldsymbol{I}$, we introduce the constitutive relations

$$\boldsymbol{\sigma}_{\text{d}} = \hat{\boldsymbol{\sigma}}_{\text{d}}(\boldsymbol{\epsilon}_{\text{d}}[\boldsymbol{v}]), \quad \boldsymbol{v} \cdot \boldsymbol{\nabla} = \hat{e}(p) \tag{3.1}$$

Hence, $\hat{\boldsymbol{\sigma}}_{\text{d}}(\bullet)$ and $\hat{e}(\bullet)$ denote suitable constitutive functions. In the simplest case of a viscous fluid, we have $\hat{\boldsymbol{\sigma}}_{\text{d}}(\boldsymbol{d}_{\text{d}}) = 2\mu\boldsymbol{d}_{\text{d}}$ and $\hat{e}(p) = -Cp$, where the material parameters $\mu(\boldsymbol{x}), C(\boldsymbol{x})$ for $\boldsymbol{x} \in \Omega^{\text{part}}$ may fluctuate strongly. Moreover, intrinsic incompressibility is defined as $\hat{e}(p) = 0$ for any value of p. In the case of flow problems, $C = 0$ is the only reasonable choice, however, the more general form is kept to illustrate the similarity between the fine-scale and macro-scale problem.

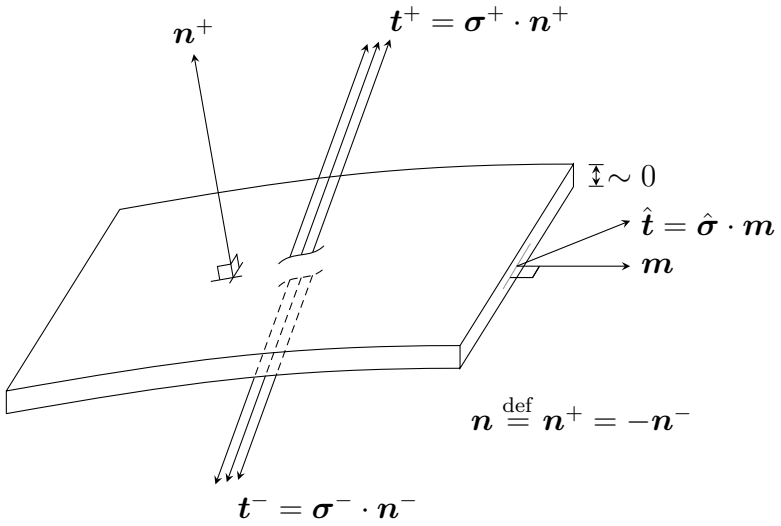

Figure 3.2: *Thin shell representing a surface with in-plane forces due to "surface tension".*

A vital part of the simulation is the modeling of surface tension, which acts as the "driving force" for liquid-phase sintering. An extensive theory on boundary energy potentials has been developed by Steinmann [Ste08], which has served as the basis for the surface tension modeling in this work. In short; equilibrium across a surface $\mathcal{S}$ represented by a thin shell bounded by the curve $\mathcal{C}$, as in Figure 3.2, can be stated as:

$$\boldsymbol{t}^+ + \boldsymbol{t}^- + \boldsymbol{t}_{\text{s}} = \boldsymbol{0} \quad \text{on } \mathcal{S} \quad \text{with } \boldsymbol{t}_{\text{s}} \stackrel{\text{def}}{=} \hat{\boldsymbol{\sigma}} \cdot \hat{\boldsymbol{\nabla}} \tag{3.2}$$

$$\sum_i \hat{\boldsymbol{t}}_i = \boldsymbol{0} \quad \text{on } \mathcal{C} \tag{3.3}$$

where $\hat{\boldsymbol{\nabla}} \stackrel{\text{def}}{=} \boldsymbol{\nabla} - [\boldsymbol{\nabla} \cdot \boldsymbol{n}]\boldsymbol{n}$ is the surface gradient. For an isotropic surface potential one obtains $\hat{\boldsymbol{\sigma}} = \gamma_{\text{s}}[\boldsymbol{I} - \boldsymbol{n} \otimes \boldsymbol{n}]$, and the common expression for the surface traction representing surface

tension is obtained:

$$\boldsymbol{t}_{\mathrm{s}} = -\kappa\gamma_{\mathrm{s}}\boldsymbol{n} \tag{3.4}$$

where $\kappa \overset{\text{def}}{=} \boldsymbol{n}\cdot\hat{\boldsymbol{\nabla}}$ is the Gaussian curvature.

We are now in the position to formulate the strong format of the fine-scale problem under standard quasistatic conditions:

$$-\left[\hat{\boldsymbol{\sigma}}_{\mathrm{d}}(\boldsymbol{\epsilon}_{\mathrm{d}}[\boldsymbol{v}]) - p\boldsymbol{I}\right]\cdot\boldsymbol{\nabla} = \boldsymbol{f} \quad \text{in } \Omega^{\mathrm{part}} \tag{3.5a}$$

$$-\boldsymbol{v}\cdot\boldsymbol{\nabla} + \hat{e}(p) = 0 \quad \text{in } \Omega^{\mathrm{part}} \tag{3.5b}$$

$$\boldsymbol{v} = \boldsymbol{v}_{\mathrm{pre}} \text{ on } \Gamma^{\mathrm{D}} \tag{3.5c}$$

$$\boldsymbol{t} \overset{\text{def}}{=} \left[\hat{\boldsymbol{\sigma}}_{\mathrm{d}}(\boldsymbol{\epsilon}_{\mathrm{d}}[\boldsymbol{v}]) - p\boldsymbol{I}\right]\cdot\boldsymbol{n} = \boldsymbol{t}_{\mathrm{pre}} \text{ on } \Gamma^{\mathrm{N}} \tag{3.5d}$$

$$\boldsymbol{t} \overset{\text{def}}{=} \left[\hat{\boldsymbol{\sigma}}_{\mathrm{d}}(\boldsymbol{\epsilon}_{\mathrm{d}}[\boldsymbol{v}]) - p\boldsymbol{I}\right]\cdot\boldsymbol{n} = \boldsymbol{t}_{\mathrm{s}} \text{ on } \Gamma^{\mathrm{pore}} \tag{3.5e}$$

The corresponding weak format is: Find $\boldsymbol{v}\in\mathbb{V}, p\in\mathbb{P}$ s.t.

$$a(\boldsymbol{v};\delta\boldsymbol{v}) + b(p,\delta\boldsymbol{v}) = l^{\mathrm{pore}}(\delta\boldsymbol{v}) + l(\delta\boldsymbol{v}) \quad \forall\delta\boldsymbol{v}\in\mathbb{V}^0 \tag{3.6a}$$

$$b(\delta p,\boldsymbol{v}) + c^*(p;\delta p) = 0 \quad \forall\delta p\in\mathbb{P} \tag{3.6b}$$

where $\mathbb{V}$ and $\mathbb{V}^0$ denotes the trial and test spaces for the velocity, respectively, $\mathbb{P}$ is the trial and test space for the pressure field, and the introduced forms are defined as

$$a(\boldsymbol{v};\boldsymbol{w}) \overset{\text{def}}{=} \int_{\Omega^{\mathrm{part}}} \boldsymbol{\epsilon}_{\mathrm{d}}[\boldsymbol{w}] : \hat{\boldsymbol{\sigma}}_{\mathrm{d}}(\boldsymbol{\epsilon}_{\mathrm{d}}[\boldsymbol{v}])\,\mathrm{d}V \tag{3.7}$$

$$b(q,\boldsymbol{v}) \overset{\text{def}}{=} -\int_{\Omega^{\mathrm{part}}} q\,\boldsymbol{v}\cdot\boldsymbol{\nabla}\,\mathrm{d}V \tag{3.8}$$

$$c^*(q;r) \overset{\text{def}}{=} \int_{\Omega^{\mathrm{part}}} r\,\hat{e}(q)\,\mathrm{d}V \tag{3.9}$$

$$l^{\mathrm{pore}}(\boldsymbol{v}) \overset{\text{def}}{=} -\int_{\Gamma^{\mathrm{pore}}} \gamma_{\mathrm{s}}\hat{\boldsymbol{I}} : [\boldsymbol{v}\otimes\boldsymbol{\nabla}]\,\mathrm{d}S \tag{3.10}$$

$$l(\boldsymbol{v}) \overset{\text{def}}{=} \int_{\Omega^{\mathrm{part}}} \boldsymbol{v}\cdot\boldsymbol{f}\,\mathrm{d}V + \int_{\Gamma^{\mathrm{N}}} \boldsymbol{v}\cdot\boldsymbol{t}_{\mathrm{pre}}\,\mathrm{d}S \tag{3.11}$$

Here, the term pertaining to surface tension, $l^{\mathrm{pore}}(\bullet)$, was obtained from eq. (3.2) and eq. (3.3) using the surface divergence theorem, cf. Paper A.

3.2 Numerical aspects

The mixed $(\boldsymbol{v},p)$-formulation requires some form of stabilized approximation for use with FEM. In this thesis, Taylor-Hood elements (quadratic velocity, linear velocity) and Mini-elements (linear pressure, linear approximation enriched by a bubble function for the velocity) have been implemented. Surface tension has been implemented according to eq. (3.10).

During the FE-simulation, the mesh eventually becomes very distorted, in particular at sharp corners subjected to surface tension. In order to approach full density, pores need to shrink to the point of vanishing. A remeshing strategy was developed in Paper A to deal with

this issue. The assumption of viscous flow alleviates part of the problem, as there are no state variables to map to the new mesh. Only the updated surfaces need to be tracked. However, that alone represents a considerable computational effort since multiple phases and boundary conditions are present.

4 Formulation of the two-scale problem

4.1 Preliminaries

As the amount of detail in the fine scale problem becomes excessive, it is advantageous to use homogenization. Variationally Consistent Homogenization (VCH) will be used to obtain the two-scale problem, as illustrated in Figure 4.1. A general review of VCH can be found in Appendix A of Paper C. In the presence of pores, the pertinent volume averaging operators are

$$\langle \bullet \rangle_\square \stackrel{\text{def}}{=} \frac{1}{|\Omega_\square|} \int_{\Omega_\square^{\text{part}}} \bullet \, \mathrm{d}V, \quad \Omega_\square^{\text{part}} \stackrel{\text{def}}{=} \Omega_\square \cap \Omega^{\text{part}} \tag{4.1}$$

$$\langle\!\langle \bullet \rangle\!\rangle_\square \stackrel{\text{def}}{=} \frac{1}{|\Omega_\square|} \int_{\Gamma_\square^{\text{pore}}} \bullet \, \mathrm{d}S, \quad \Gamma_\square^{\text{pore}} \stackrel{\text{def}}{=} \Omega_\square \cap \Gamma^{\text{pore}} \tag{4.2}$$

where $\Omega_\square$ is the "window" of the Representative Volume Element (RVE) as illustrated in Figure 4.1 and Figure 4.2. At the macroscale, the homogenized properties from solving the RVE-problems replace the material model.

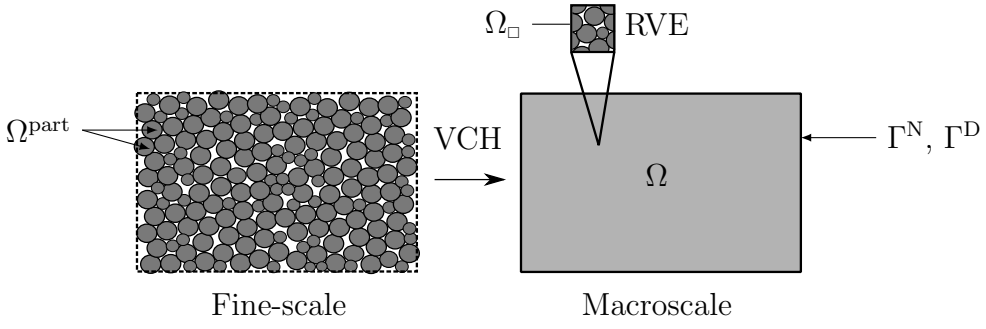

Figure 4.1: *Homogenization of a "green body". Particles are not to scale.*

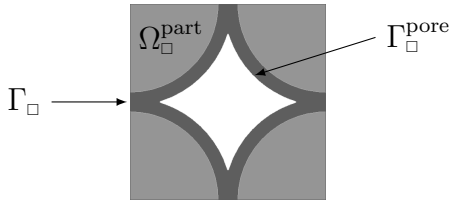

Figure 4.2: *Example of an idealized RVE consisting of a single unit cell of spherical particles in contact.*

At the core of VCH is the hierarchical split of the unknown primary fields. In the present case we have two fields, $\boldsymbol{v}$ and p, which we decompose into macroscopic and fluctuating parts,

$\boldsymbol{v} = \boldsymbol{v}^{\mathrm{M}} + \boldsymbol{v}^{\mathrm{s}}$ and $p = p^{\mathrm{M}} + p^{\mathrm{s}}$, and depending on how these are chosen different macroscale and RVE-problems are obtained.

When using VCH, one also wishes to preserve typical Galerkin properties, such as symmetry of the macroscale tangent operators. Therefore, it is crucial also to satisfy the Variationally Consistent Macrohomogeneity Condition (VCMC). In the appended papers, a VCMC is indeed satisfied, and it can be recognized as a generalized Hill-Mandel condition.

4.2 VCH for the macroscopically compressible case

In Paper A, the following modeling assumptions are introduced for the macroscale fields $\boldsymbol{v}^{\mathrm{M}}$ and p^{M} within each RVE: First order Taylor expansion of the velocity, and no macroscale pressure, i.e.

$$\boldsymbol{v}^{\mathrm{M}} = \bar{\boldsymbol{v}} + [\bar{\boldsymbol{v}} \otimes \boldsymbol{\nabla}] \cdot [\boldsymbol{x} - \bar{\boldsymbol{x}}] \tag{4.3}$$

$$p^{\mathrm{M}} = 0 \tag{4.4}$$

A constraint on the fluctuation $\boldsymbol{v}^{\mathrm{s}}$ within each RVE is imposed via the condition

$$\frac{1}{|\Omega_{\square}|} \int_{\Gamma_{\square}} \boldsymbol{v} \otimes \boldsymbol{n} \, \mathrm{d}S = \bar{\boldsymbol{v}} \otimes \boldsymbol{\nabla} \tag{4.5}$$

As a consequence, the macroscale problem is obtained as follows: Solve for $\bar{\boldsymbol{v}}$ from

$$-\bar{\boldsymbol{\sigma}}\{\bar{\boldsymbol{d}}\} \cdot \boldsymbol{\nabla} = \bar{\boldsymbol{f}} \quad \text{in } \Omega \tag{4.6a}$$

$$\bar{\boldsymbol{v}} = \bar{\boldsymbol{v}}_{\mathrm{pre}} \text{ on } \Gamma_{\mathrm{D}} \tag{4.6b}$$

$$\bar{\boldsymbol{t}} = \bar{\boldsymbol{t}}_{\mathrm{pre}} \text{ on } \Gamma_{\mathrm{N}} \tag{4.6c}$$

where $\bar{\boldsymbol{d}} \overset{\mathrm{def}}{=} [\bar{\boldsymbol{v}} \otimes \boldsymbol{\nabla}]^{\mathrm{sym}}$ and $\bar{\boldsymbol{\sigma}}$ is the homogenized response (derived by VCH) from the RVE-problem. It is noted that only the velocity exists as a primary field at the macroscale.

The RVE-problem with Dirichlet boundary conditions becomes: For given $\bar{\boldsymbol{d}}$, compute $(\boldsymbol{v}, p)$ from

$$-[\hat{\boldsymbol{\sigma}}_{\mathrm{d}}(\boldsymbol{\epsilon}_{\mathrm{d}}[\boldsymbol{v}]) - p\boldsymbol{I}] \cdot \boldsymbol{\nabla} = \boldsymbol{f} \quad \text{in } \Omega_{\square}^{\mathrm{part}} \tag{4.7a}$$

$$-\boldsymbol{v} \cdot \boldsymbol{\nabla} + \hat{e}(p) = 0 \quad \text{in } \Omega_{\square}^{\mathrm{part}} \tag{4.7b}$$

$$\boldsymbol{v} = \bar{\boldsymbol{d}} \cdot [\boldsymbol{x} - \bar{\boldsymbol{x}}] \text{ on } \Gamma_{\square} \tag{4.7c}$$

$$\boldsymbol{t} = \boldsymbol{t}_{\mathrm{s}} \quad \text{on } \Gamma_{\square}^{\mathrm{pore}} \tag{4.7d}$$

Unfortunately, the theory breaks down at the macroscopically incompressible limit, where the entire macroscopic rate-of-deformation tensor, $\bar{\boldsymbol{d}}$, can no longer be directly controlled, as the bulk stiffness tends to infinity.

4.3 VCH with seamless transition to the macroscopically incompressible case

In Paper C, the model assumptions for the macroscopic fields are as follows: First order Taylor expansion of the velocity (or displacement), and zeroth order expansion for the pressure

$$\boldsymbol{v}^{\mathrm{M}} = \bar{\boldsymbol{v}} + [\bar{\boldsymbol{v}} \otimes \boldsymbol{\nabla}] \cdot [\boldsymbol{x} - \bar{\boldsymbol{x}}] \tag{4.8}$$

$$p^{\mathrm{M}} = \bar{p} \tag{4.9}$$

Constraints on the fluctuations $\boldsymbol{v}^{\mathrm{s}}$ and p^{s} within each RVE are imposed via the requirements

$$\langle \boldsymbol{v} \otimes \boldsymbol{\nabla} \rangle_{\square} = \bar{\boldsymbol{v}} \otimes \boldsymbol{\nabla} \tag{4.10}$$

$$\langle p \rangle_{\square} = \bar{p} \tag{4.11}$$

This leads to a macroscale problem in the mixed format: Solve for $(\bar{\boldsymbol{v}}, \bar{p})$ from

$$-[\bar{\boldsymbol{\sigma}}_{\mathrm{d}}\{\bar{\boldsymbol{d}}_{\mathrm{d}}, \bar{p}\} - \bar{p}\boldsymbol{I}] \cdot \boldsymbol{\nabla} = \bar{\boldsymbol{f}} \quad \text{in } \Omega \tag{4.12a}$$

$$-\bar{\boldsymbol{v}} \cdot \boldsymbol{\nabla} + \bar{e}\{\bar{\boldsymbol{d}}_{\mathrm{d}}, \bar{p}\} = 0 \quad \text{in } \Omega \tag{4.12b}$$

$$\bar{\boldsymbol{v}} = \bar{\boldsymbol{v}}_{\mathrm{pre}} \text{ on } \Gamma_{\mathrm{D}} \tag{4.12c}$$

$$\bar{\boldsymbol{t}} = \bar{\boldsymbol{t}}_{\mathrm{pre}} \text{ on } \Gamma_{\mathrm{N}} \tag{4.12d}$$

where $\bar{\boldsymbol{d}}_{\mathrm{d}} = \boldsymbol{\epsilon}_{\mathrm{d}}[\bar{\boldsymbol{v}}]$ and $(\bar{\boldsymbol{\sigma}}_{\mathrm{d}}, \bar{e})$ are the homogenized response variables (derived by VCH) from the RVE-problem. The intentional similarity of (4.12) and (3.5a)–(3.5d) is emphasized. This mixed formulation is capable of seamless transition to the incompressible response, which is identified by $\bar{e} = 0$.

However, in the case when pores and surface tension are present, as in Paper D, it is necessary to choose the prolongation assumption for the pressure in a non-standard fashion

$$\boldsymbol{v}^{\mathrm{M}} = \bar{\boldsymbol{v}} + [\bar{\boldsymbol{v}} \otimes \boldsymbol{\nabla}] \cdot [\boldsymbol{x} - \bar{\boldsymbol{x}}] \tag{4.13}$$

$$p^{\mathrm{M}} = \frac{|\Omega_{\square}|}{|\Omega_{\square}^{\mathrm{part}}|}[\bar{p} + \frac{2}{3}\langle\langle \gamma_{\mathrm{s}} \rangle\rangle_{\square}] \tag{4.14}$$

The requirements on the fluctuations within each RVE are now formulated as

$$\frac{1}{|\Omega_{\square}|} \int_{\Gamma_{\square}} \boldsymbol{v} \otimes \boldsymbol{n} \, \mathrm{d}S = \bar{\boldsymbol{v}} \otimes \boldsymbol{\nabla} \tag{4.15}$$

$$\langle p \rangle_{\square} - \frac{2}{3}\langle\langle \gamma_{\mathrm{s}} \rangle\rangle_{\square} = \bar{p} \tag{4.16}$$

With these choices, it is possible to maintain the macroscale problem in eq. (4.12), as shown in detail in Paper D.

As an example, the RVE-problem with Dirichlet boundary conditions now becomes: For given $(\bar{\boldsymbol{d}}_{\mathrm{d}}, \bar{p})$, compute $(\boldsymbol{v}, p, \bar{e})$ from

$$-[\hat{\boldsymbol{\sigma}}_{\mathrm{d}}(\boldsymbol{\epsilon}_{\mathrm{d}}[\boldsymbol{v}]) - p\boldsymbol{I}] \cdot \boldsymbol{\nabla} = \boldsymbol{f} \quad \text{in } \Omega_{\square}^{\mathrm{part}} \tag{4.17a}$$

$$-\boldsymbol{v} \cdot \boldsymbol{\nabla} + \hat{e}(p) = 0 \quad \text{in } \Omega_{\square}^{\mathrm{part}} \tag{4.17b}$$

$$\langle p \rangle_{\square} = \frac{2}{3}\langle\langle \gamma_{\mathrm{s}} \rangle\rangle_{\square} + \bar{p} \tag{4.17c}$$

$$\boldsymbol{v} - \frac{1}{3}\bar{e}\,[\boldsymbol{x} - \bar{\boldsymbol{x}}] = \bar{\boldsymbol{d}}_{\mathrm{d}} \cdot [\boldsymbol{x} - \bar{\boldsymbol{x}}] \text{ on } \Gamma_{\square} \tag{4.17d}$$

$$\boldsymbol{t} = \boldsymbol{t}_{\mathrm{s}} \quad \text{on } \Gamma_{\square}^{\mathrm{pore}} \tag{4.17e}$$

Other possibilities are Neumann and weakly periodic boundary conditions for the RVE-problem, which are elaborated in Paper D.

As an alternative, the procedure in Paper B represents pure algebraic manipulations to rewrite eq. (4.6) in order to enable the transition to the macroscopically incompressible limit. The used strategy is to replace the step $\bar{\boldsymbol{d}} \rightarrow \bar{\boldsymbol{\sigma}}$ by mixed control for the RVE-problem $(\bar{\boldsymbol{d}}_{\mathrm{d}}, \bar{p}) \rightarrow (\bar{\boldsymbol{\sigma}}_{\mathrm{d}}, \bar{e})$. As the result from this manipulation, one obtains exactly the macroscale problem and the RVE-problem described in eq. (4.12) and eq. (4.17) respectively.

The mixed macroscopic $(\bar{\boldsymbol{v}}, \bar{p})$-formulation in eq. (4.12) will also require stabilization and the Taylor-Hood approximation is the obvious choice. The RVE-problem also requires unusual boundary conditions, as seen in eq. (4.17d), and therefore requires a flexible finite element code for implementation. The FE^2 algorithm is available in the open source code OOFEM (cf. [Pat00]).

5 Summary of Appended Papers

- **Paper A: Computational mesoscale modeling and homogenization of liquid-phase sintering of particle agglomerates**. Liquid phase sintering of particle agglomerates is simulated as the viscous deformation of particle-particle contact, whereby the single driving force is the surface tension on the particle/pore interface. Particles are modeled as purely viscous fluids (with no elasticity). Computational homogenization is adopted for the RVE with Dirichlet boundary conditions. A surface motion algorithm is developed that requires complete remeshing of the FE-mesh based on a "maximum deformation" criterion. Since the particles are intrinsically incompressible, the macroscopic compressibility is determined from shrinking porosity in the substructure.

  The numerical examples include free sintering of an RVE and a fully coupled FE^2-simulation of a specimen with inhomogeneous initial distribution of porosity.

  The FE^2-format (only valid for macroscopic compressibility) for the Dirichlet boundary condition is summarized in the following flowchart

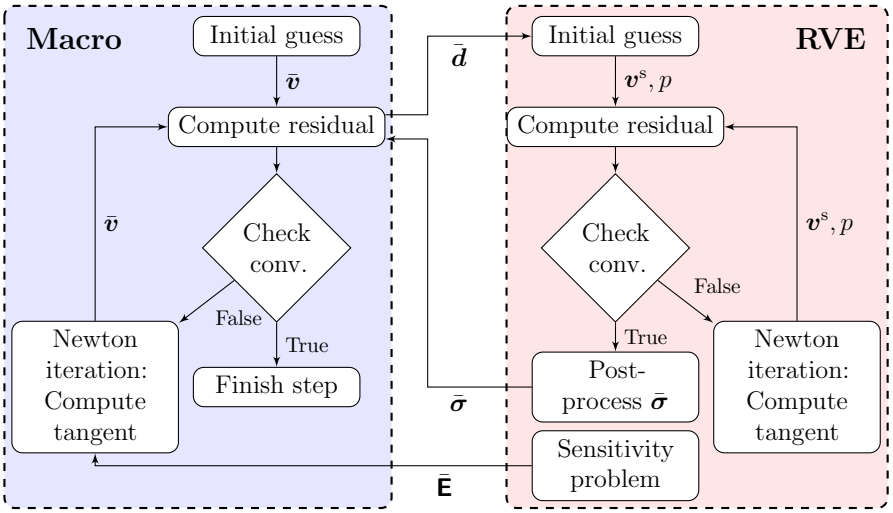

- **Paper B: Computational homogenization of liquid-phase sintering with seamless transition from macroscopic compressibility to incompressibility**. Liquid

phase sintering of particle agglomerates is modeled on the mesoscale as the viscous deformation of particle-particle contact, whereby the single driving force is the surface tension on the particle/pore interface. On the macroscale, a quasistatic equilibrium problem allows for the prediction of the shrinkage of the sintering body. The present paper presents a novel FE^2 formulation of the two-scale sintering problem allowing for the transition to zero porosity, implying macroscale incompressibility. The seamless transition from compressibility to incompressibility on the macroscale is accomplished by introducing a mixed variational format of the macroscale problem. This has consequences also for the formulation of the mesoscale problem, that is complemented with an extra constraint equation regarding the prolongation of the volumetric part of the macroscopic rate-of-deformation.

The numerical example shows the sintering of a single Representative Volume Element (RVE), which is sheared beyond the point where the porosity vanishes while subjected to zero macroscopic pressure.

The FE^2-format (modified to handle seamless transition from macroscopic compressibility to incompressibility) for the Dirichlet boundary condition is summarized in the following flowchart

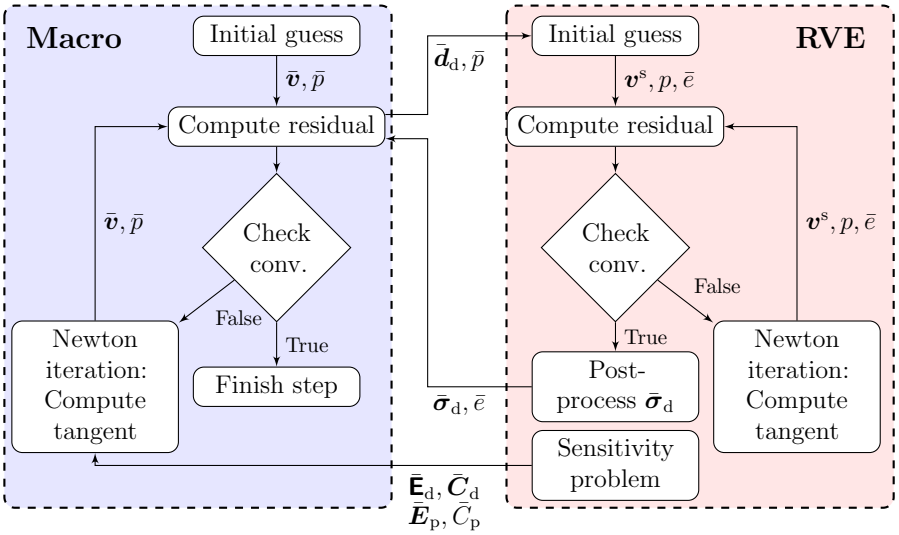

- **Paper C: On the variationally consistent computational homogenization of elasticity in the incompressible limit**. In this work, a mixed displacement-pressure formulation for elasticity is considered as the prototype problem. Variationally Consistent Homogenization (VCH) is directly used to derive the macroscale problem, and the Variationally Consistent Macrohomogeneity Condition (VCMC) is used to determine the RVE-problem. Dirichlet, Neumann, and (weakly) periodic boundary conditions for the RVE's are derived, and it is shown that the Dirichlet and Neumann boundary conditions provide bounds for the periodic boundary condition in terms of effective stiffness.

  The numerical examples show the convergence rate of the Neumann and Dirichlet boundary conditions for a series of 3D Statistical Volume Elements (SVE's). A final example shows the influence of the compressibility of the microconstituents on the homogenized macroscopic shear modulus.

The FE^2-format for the weakly periodic boundary condition is summarized in the following flowchart

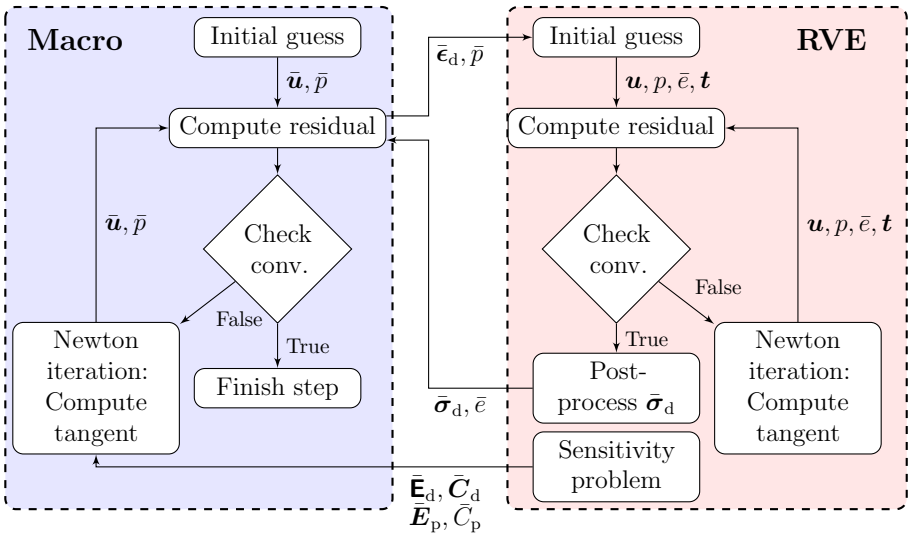

- **Paper D: A mixed variational format for two-scale analysis of liquid-phase sintering based on variationally consistent homogenization**. The final work in this thesis combines the Variationally Consistent Homogenization strategy presented in Paper C with the mesoscale modeling in Paper A and Paper B. In particular, it is shown that the Dirichlet boundary condition becomes equivalent to that in Paper C. Also highlighted in this paper is that the surface tension may obtain an additional contribution to the deviatoric part of the macroscopic stress, whereas traditional models for sintering only accounts for volumetric macroscopic "sintering stress". The deviatoric contribution to the macroscopic stress is naturally captured by the RVE-problems as part of the homogenization procedure.

The numerical examples show the transient behavior of the Neumann and Dirichlet boundary conditions for a 2D RVE subject to free sintering. The effective macroscale properties of the Dirichlet, Neumann and weakly periodic boundary condition are compared for a 3D microstructure.

The FE^2-format for the weakly periodic boundary condition is summarized in the following flowchart

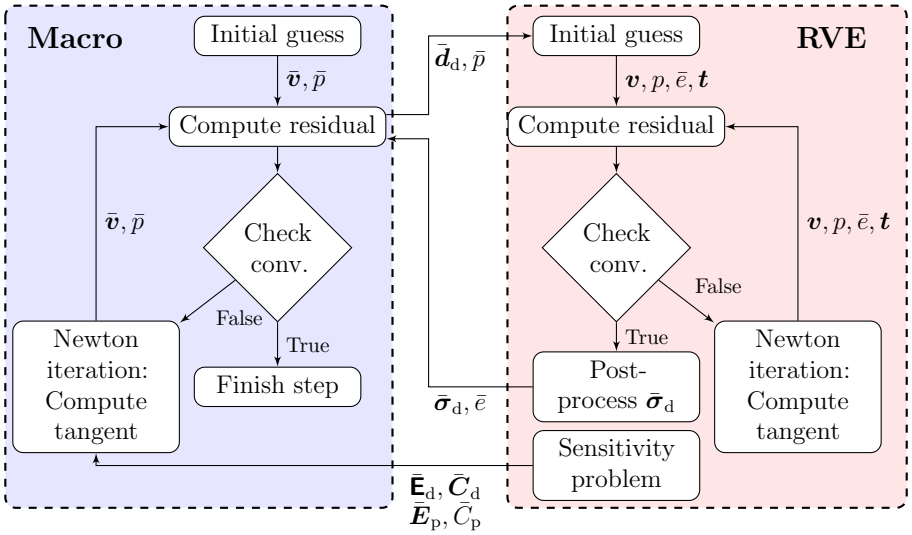

6 Contributions of the thesis

- In Paper A and the extension in Paper B, we find the first variationally consistent multiscale problem for sintering. In Paper B the procedure is extended into the macroscopically incompressible regime. Numerical investigations show how the pore shape strongly influences the "sintering stress".

- To deal with large topological changes in the RVE-problems, a surface tracking algorithm capable of tracking multiple phases, allowing for vanishing pores and the tracking multiple regions for boundary conditions, was implemented for Paper A. This allow for the Lagrangian mesh to follow the free surface flow of the sintered particles to the point of vanishing porosity, as the FE^2-simulations in Paper B demonstrates.

- In Paper C, VCH is applied to elasticity in mixed $(\boldsymbol{u}, p)$-formulation for the first time. Numerical examples investigate the influence of bulk modulus of constituents (to the point of macroscopic incompressibility) on the homogenized shear modulus.

- The weakly periodic, Dirichlet, and Neumann boundary conditions for the RVEs under mixed $(\bar{\boldsymbol{d}}_{\mathrm{d}}, \bar{p})$-control are derived for the first time.

- Finalizing the thesis with Paper D, we find VCH applied to mixed formulation, allowing for incompressibility and existence of pore space with surface tension.

7 Concluding remarks and Future work

In this thesis a novel approach to simulate the sintering process as a problem of computational homogenization is presented, replacing traditional (macroscopic) constitutive modeling. With the proposed homogenization procedure, a seamless transition from the macroscopically compressible to the incompressible response is ensured, which is of vital importance when modeling sintering of particle composites.

Through rigorously applying VCH, we can ensure that the obtained macroscale problem is sound, and the RVE-problem retains the same strong form as the fine scale problem. These properties allow for a straightforward FE-implementation.

For the homogenization procedure, pores on the RVE-boundaries remain complicated. Weakly periodic and Neumann boundary conditions are not applicable, while Dirichlet boundary conditions constrains the closing of pores on the boundary. A strongly periodic boundary condition could therefore be a necessity for RVEs with pores intersecting the boundary, but makes it considerably harder to (re)generate a mesh.

There are also possible improvements of the subscale modeling, where the bulk- and surface-diffusion is still missing. Due to limitations in the remeshing and post-processing software, the microstructural properties of the "green body", i.e. before the sintering process starts, have so far only been idealized to contacting spheres. While these serve the need for demonstrating the homogenization procedure, they fail to capture a realistic microstructure of many typical sintered products.

An attempt to address the large topological changes have been outlined in Paper A, but is lacking a robust 3D implementation. Alternative methods such as level sets, volume fractions, or particle-FEM could offer a simpler numerical procedure for the fine-scale problem.

References

[Bie+04] C. Bient et al. Modeling of distortion after densification during liquid-phase sintering. *Metallurgical and Materials Transactions A* **35**.12 (Dec. 2004), 3833–3841. ISSN: 1073-5623. DOI: 10.1007/s11661-004-0289-z.

[BN98] J. Brandt and L. Nilsson. FE-Simulation of compaction and solid-state sintering of cemented carbides. *Mechanics of Cohesive-frictional Materials* **3**.2 (Apr. 1998), 181–205. ISSN: 1082-5010. DOI: 10.1002/(SICI)1099-1484(199804)3:2<181::AID-CFM47>3.0.CO;2-H.

[DP06] W. G. Dettmer and D. Perić. A computational framework for free surface fluid flows accounting for surface tension. *Computer Methods in Applied Mechanics and Engineering* **195**.23-24 (2006), 3038–3071. ISSN: 00457825. DOI: 10.1016/j.cma.2004.07.057.

[FC00] F. Feyel and J.-L. Chaboche. FE2 multiscale approach for modelling the elastoviscoplastic behaviour of long fibre SiC/Ti composite materials. *Computer Methods in Applied Mechanics and Engineering* **183**.3–4 (Mar. 2000), 309–330. ISSN: 0045-7825. DOI: 10.1016/S0045-7825(99)00224-8.

[FKM92] N. A. Fleck, L. T. Kuhn, and R. M. McMeeking. Yielding of metal powder bonded by isolated contacts. *Journal of the Mechanics and Physics of Solids* **40**.5 (July 1992), 1139–1162. ISSN: 00225096. DOI: 10.1016/0022-5096(92)90064-9.

[Ger96] R. M. German. *Sintering theory and practice*. Wiley, 1996. ISBN: 0-471-05786-X. URL: http://adsabs.harvard.edu/abs/1996stp..book.....G.

[GKB10] M. G. D. Geers, V. G. Kouznetsova, and W. A. M. Brekelmans. Multi-scale computational homogenization: Trends and challenges. *Journal of Computational and Applied Mathematics* **234**.7 (Aug. 2010), 2175–2182. ISSN: 0377-0427. DOI: 10.1016/j.cam.2009.08.077.

[HEA85] A. S. Helle, K. E. Easterling, and M. F. Ashby. Hot-isostatic pressing diagrams: New developments. *Acta Metallurgica* **33**.12 (Dec. 1985), 2163–2174. ISSN: 00016160. DOI: 10.1016/0001-6160(85)90177-4.

[JD88a] A. Jagota and P. R. Dawson. Micromechanical modeling of powder compacts — II. Truss formulation of discrete packings. *Acta Metallurgica* **36**.9 (Sept. 1988), 2563–2573. ISSN: 00016160. DOI: 10.1016/0001-6160(88)90201-5.

[JD88b] A. Jagota and P. R. Dawson. Micromechanical modeling of powder compacts — I. Unit problems for sintering and traction induced deformation. *Acta Metallurgica* **36**.9 (Sept. 1988), 2551–2561. ISSN: 00016160. DOI: 10.1016/0001-6160(88)90200-3.

[JS10] A. Javili and P. Steinmann. A finite element framework for continua with boundary energies. Part II: The three-dimensional case. *Computer Methods in Applied Mechanics and Engineering* **199**.9-12 (Jan. 2010), 755–765. ISSN: 00457825. DOI: 10.1016/j.cma.2009.11.003.

[Kra03] T. Kraft. Optimizing press tool shapes by numerical simulation of compaction and sintering application to a hard metal cutting insert. *Modelling and Simulation in Materials Science and Engineering* **11**.3 (May 2003), 381–400. ISSN: 0965-0393. DOI: 10.1088/0965-0393/11/3/310.

[LRS10] F. Larsson, K. Runesson, and F. Su. Variationally consistent computational homogenization of transient heat flow. *International Journal for Numerical Methods in Engineering* **81**.13 (Mar. 2010), 1659–1686. ISSN: 00295981. DOI: 10.1002/nme.2747.

[Lu+01] P. Lu et al. Porosity effect on densification and shape distortion in liquid phase sintering. *Materials Science and Engineering A* **318**.1-2 (Nov. 2001), 111–121. ISSN: 09215093. DOI: 10.1016/S0921-5093(01)01330-2.

[Luq+05] A. Luque et al. Simulation of the microstructural evolution during liquid phase sintering using a geometrical Monte Carlo model. *Modelling and Simulation in Materials Science and Engineering* **13**.7 (Oct. 2005), 1057–1070. ISSN: 0965-0393. DOI: 10.1088/0965-0393/13/7/004.

[MK92] R. M. McMeeking and L. T. Kuhn. A diffusional creep law for powder compacts. *Acta Metallurgica et Materialia* **40**.5 (May 1992), 961–969. ISSN: 09567151. DOI: 10.1016/0956-7151(92)90073-N.

[MR00] L. Mähler and K. Runesson. Modelling of solid-phase sintering of hardmetal using a mesomechanics approach. *Mechanics of Cohesive-frictional Materials* **5**.8 (Nov. 2000), 653–671. ISSN: 1082-5010. DOI: 10.1002/1099-1484(200011)5:8<653::AID-CFM111>3.0.CO;2-A.

[MR03] L. Mähler and K. Runesson. Constitutive modeling of cold compaction and sintering of hardmetal. *Journal of Engineering Materials and Technology* **125**.2 (2003), 191. ISSN: 00944289. DOI: 10.1115/1.1491576.

[NH93] S. Nemat-Nasser and M. Hori. *Micromechanics: Overall properties of heterogeneous materials*. Elsevier, 1993. ISBN: 978-0-444-50084-7.

[OG00] E. A. Olevsky and R. M. German. Effect of gravity on dimensional change during sintering - I. Shrinkage anisotropy. English. *Acta Materialia* **48**.5 (2000), 1153–1166. ISSN: 1359-6454. DOI: 10.1016/S1359-6454(99)00368-7.

[Öhm14] M. Öhman. A mixed variational format for two-scale analysis of liquid-phase sintering based on variationally consistent homogenization (2014). In preparation.

[Ole98] E. A. Olevsky. Theory of sintering: from discrete to continuum. *Materials Science and Engineering: R: Reports* **23**.2 (June 1998), 41–100. ISSN: 0927-796X. DOI: 10.1016/S0927-796X(98)00009-6.

[OOC96] J. Oliver, S. Oller, and J. C. Cante. A plasticity model for simulation of industrial powder compaction processes. *International Journal of Solids and Structures* **33**.20-22 (Aug. 1996), 3161–3178. ISSN: 00207683. DOI: 10.1016/0020-7683(95)00249-9.

[ÖRL12] M. Öhman, K. Runesson, and F. Larsson. Computational mesoscale modeling and homogenization of liquid-phase sintering of particle agglomerates. *Technische Mechanik* **32** (2012),

463–483. ISSN: 0232-3869. URL: http://www.uni-magdeburg.de/ifme/zeitschrift_tm/2012_Heft2_5/33_Oehman.pdf.

[ÖRL13] M. Öhman, K. Runesson, and F. Larsson. Computational homogenization of liquid-phase sintering with seamless transition from macroscopic compressibility to incompressibility. *Computer Methods in Applied Mechanics and Engineering* **266** (2013), 219–228. ISSN: 0045-7825. DOI: 10.1016/j.cma.2013.07.006.

[ÖRL14] M. Öhman, K. Runesson, and F. Larsson. On the variationally consistent computational homogenization of elasticity in the incompressible limit. *Advanced Modeling and Simulation in Engineering Sciences* (2014). Submitted.

[Pat00] B. Patzák. *OOFEM project home page*. 2000. URL: http://www.oofem.org.

[Pin+13] D. Pino Muñoz et al. Direct 3D simulation of powder sintering by surface and volume diffusion. *Key Engineering Materials* **554-557** (June 2013), 714–723. ISSN: 1662-9795. DOI: 10.4028/www.scientific.net/KEM.554-557.714.

[Red98] P. Redanz. Numerical modelling of cold compaction of metal powder. *International Journal of Mechanical Sciences* **40**.11 (Nov. 1998), 1175–1189. ISSN: 00207403. DOI: 10.1016/S0020-7403(98)00021-6.

[RO90] C. R. Reid and R. G. Oakberg. A continuum theory for the mechanical response of materials to the thermodynamic stress of sintering. *Mechanics of Materials* **10**.3 (Dec. 1990), 203–213. ISSN: 01676636. DOI: 10.1016/0167-6636(90)90043-F.

[RS93] H. Riedel and J. Svoboda. A theoretical study of grain growth in porous solids during sintering. *Acta Metallurgica et Materialia* **41**.6 (June 1993), 1929–1936. ISSN: 09567151. DOI: 10.1016/0956-7151(93)90212-B.

[Shi96] K. Shinagawa. Finite element simulation of sintering process. *JSME International Journal, Series A: Mechanics and Materials Engineering* **39** (1996), 565–572. ISSN: 1340-8046. URL: http://cat.inist.fr/?aModele=afficheN&cpsidt=2486262.

[SP06a] P. H. Saksono and D. Perić. On finite element modelling of surface tension: Variational formulation and applications – Part II: Dynamic problems. *Computational Mechanics* **38**.3 (Nov. 2006), 251–263. ISSN: 0178-7675. DOI: 10.1007/s00466-005-0745-7.

[SP06b] P. H. Saksono and D. Perić. On finite element modelling of surface tension: Variational formulation and applications – Part I: Quasistatic problems. *Computational Mechanics* **38**.3 (Nov. 2006), 265–281. ISSN: 0178-7675. DOI: 10.1007/s00466-005-0747-5.

[SR95] J. Svoboda and H. Riedel. New solutions describing the formation of interparticle necks in solid-state sintering. *Acta Metallurgica et Materialia* **43**.1 (Jan. 1995), 1–10. ISSN: 09567151. DOI: 10.1016/0956-7151(95)90255-4.

[SRG96] J. Svoboda, H. Riedel, and R. Gaebel. A model for liquid phase sintering. *Acta Materialia* **44**.8 (Aug. 1996), 3215–3226. ISSN: 13596454. DOI: 10.1016/1359-6454(95)00440-8.

[Ste08] P. Steinmann. On boundary potential energies in deformational and configurational mechanics. *Journal of the Mechanics and Physics of Solids* **56**.3 (2008), 772–800. ISSN: 00225096. DOI: 10.1016/j.jmps.2007.07.001.

[Vor93] G. A. L. van de Vorst. Integral method for a two-dimensional Stokes flow with shrinking holes applied to viscous sintering. *Journal of Fluid Mechanics* **257** (Apr. 1993), 667–689. ISSN: 0022-1120. DOI: 10.1017/S002211209300326X.

[XM97] K. Xu and M. M. Mehrabadi. A micromechanical model for the initial rearrangement stage of liquid phase sintering. *Mechanics of Materials* **25**.2 (1997), 157–137. DOI: 10.1016/S0167-6636(96)00048-8.

[ZD01] H. Zhou and J. J. Derby. An assessment of a parallel, finite element method for three-dimensional, moving-boundary flows driven by capillarity for simulation of viscous sintering. *International Journal for Numerical Methods in Fluids* **36**.7 (Aug. 2001), 841–865. ISSN: 0271-2091. DOI: 10.1002/fld.159.

[ZD98] H. Zhou and J. J. Derby. Three-dimensional fnite-element analysis of viscous sintering. *Journal of the American Ceramic Society* **81**.3 (Jan. 1998), 533–540. ISSN: 00027820. DOI: 10.1111/j.1151-2916.1998.tb02371.x.